ELSEVIER

Journal of Organometallic Chemistry 561 (1998) 57–65

Journal of Organometallic Chemistry

Mechanistic aspects of the thermal *mer*-to-*fac* isomerization of *mer*-[Mn(X)(CO)$_3$(α-diimine)] (X = Cl, Br, I)

Cornelis J. Kleverlaan, František Hartl *, Derk J. Stufkens

Anorganisch Chemisch Laboratorium, Institute of Molecular Chemistry, Universiteit van Amsterdam, Nieuwe Achtergracht 166, 1018 WV Amsterdam, The Netherlands

Received 8 November 1997

Abstract

The thermal *mer*-to-*fac* isomerization of the photochemically generated complexes *mer*-[Mn(X)(CO)$_3$(α-diimine)] (X = Cl, Br, I, α-diimine = *N*,*N*′-diisopropyl-1,4-diazabutadiene (*i*Pr-DAB); X = Br, α-diimine = 4,4′-dimethyl-2,2′-bipyridine (bpy′), pyridine-2-carbaldehyde-*N*-isopropylimine (*i*Pr-PyCa), 2,3-dipyrid-2′-ylpyrazine (dpp), and R-DAB (R = *c*Pr, *i*Pr, *t*Bu)) was investigated by real-time (RT) FTIR spectroscopy at various temperatures and in different solvents. In addition, the *fac*- and *mer*-isomers were also studied by UV–vis spectroscopy. The intricate isomerization process has been characterized by determination of (i) (pseudo) first-order rate constants from linear $\ln(A_{oo}-A_t)$ versus time plots, and (ii) the corresponding thermodynamic activation parameters $\Delta S^{\ddagger}$ and $\Delta H^{\ddagger}$ from Eyring plots. For *mer*-[Mn(Br)(CO)$_3$(bpy′)] in THF the kinetic and thermodynamic data are consistent with a mechanism which probably involves association of THF and partial dissociation of the Br^- ligand. In contrast with this, the rapid isomerization of the complexes *mer*-[Mn(X)(CO)$_3$(R-DAB)] (X = Cl, Br; R = *i*Pr, and X = Br; R = *c*Pr, *i*Pr, *t*Bu) with the highly flexible electron-withdrawing R-DAB ligands follows a dissociative course probably involving cleavage of a Mn–N bond. These major reaction pathways have been employed to explain the isomerization of the other complexes under study, viz. *mer*-[Mn(X)(CO)$_3$(α-diimine)] (X = Br; α-diimine = *i*Pr-PyCa, dpp, or X = I; α-diimine = *i*Pr-DAB).

Keywords: α-Diimine complexes; Kinetics; Manganese carbonyls; Isomerization.

1. Introduction

Transition metal complexes possessing a lowest metal-to-ligand charge transfer (MLCT) state often participate in efficient energy and electron transfer processes. Among the most studied compounds in this respect are the complexes [Re(L)(CO)$_3$(bpy)]^n ($n = 0, +1$; bpy = 2,2′-bipyridine; L = halide, O- or N-donor ligand) [1–5] and their derivatives. Their electronic spectra exhibit an intense absorption band in the near-UV–vis region attributed to MLCT transitions directed to the lowest empty π^* orbital of the α-diimine ligand. Irradiation into this MLCT band usually does not lead to a photoreaction. In marked contrast, the corresponding complexes *fac*-[Mn(X)(CO)$_3$(α-diimine)] (X = halide; α-diimine = bpy, R-PyCa, R-DAB) are highly photoreactive. At r.t. they were found to undergo the remarkable sequence of photo- and thermal reactions as summarized in Scheme 1 [6,7].

According to this mechanism, *fac*-[Mn(X)(CO)$_3$(α-diimine)] loses an equatorial CO ligand on irradiation with visible light and converts to solvent-substituted *cis*,*cis*-[Mn(X)(Sv)(CO)$_2$(α-diimine)] [6]. A similar reaction was observed for *fac*-[Mn(Me)(CO)$_3$(α-diimine)] [8]. Recent density functional calculations on *fac*-[Mn(Cl)(CO)$_3$(H-DAB)] [9], and a real-time (RT) FTIR study of the primary photoprocess [7] have revealed that the release of the equatorial CO ligand induces a concomitant shift of the chloride to the open equatorial

* Corresponding author. Tel.: +31 20 5256450; fax: +31 20 5256456.

0022-328X/98/$19.00
PII S0022-328X(98)00489-6

site. The photoproduct *cis,cis*-[Mn(X)(Sv)(CO)$_2$(α-diimine)] can subsequently react with the liberated CO molecule, to produce the isomer *mer*-[Mn(X)(CO)$_3$(α-diimine)]. Further irradiation of the latter complex results in homolytic splitting of the Mn–X bond followed by secondary reactions of the radical [Mn(CO)$_3$(α-diimine)]$^{\bullet}$. In the dark *mer*-[Mn(X)(CO)$_3$(α-diimine)] reacts thermally back to the parent *fac*-isomer [6,7].

Thermal *cis–trans* and *fac–mer* isomerization of octahedral complexes can proceed either via ligand dissociation followed by rearrangement of the five-coordinate intermediate, or via a non-bond-breaking, intramolecular mechanism. Three major alternative mechanisms have been suggested for the intramolecular rearrangement involving a trigonal-prismatic transition state; the Bailar (trigonal) twist [10] and its rigid-ring alternatives, the Rây-Dutt (rhomboid) twist [11], and the Springer–Sievers twist [12]. Another possibility is the bicapped-tetrahedron mechanism [13,14], which is however also believed to pass through the trigonal–prismatic transition state.

The *fac*-to-*mer* isomerization of the related complexes *fac*-[Mn(Br)(CO)$_3$(PR$_3$)$_2$] has been postulated to occur via a bond rupture mechanism where the corresponding *mer*-isomer is formed via a trigonal bipyramidal intermediate. In this case, the $\Delta S^{\ddagger}$ values are always positive, as expected for a dissociative process [15]. It is noteworthy that no *mer*-to-*fac* isomerization was observed for *mer*-[Mn(X)(CO)$_3$(L-L)] (L-L = bidentate phosphine or arsine) though the *fac*-isomer is thermodynamically favored. In contrast to this, facile *fac*-to-*mer* isomerization occurred in the case of the oxidized complexes *fac*-[Mn(X)(CO)$_3$(L-L)]$^+$ [16]. For L-L = diphosphine ligand this reaction probably proceeds via a twist mechanism, as judged from the negative $\Delta S^{\ddagger}$ values and the limited substituent and solvent dependence of the reaction rates. On the other hand, the presence of bulky diarsine ligands in *fac*-[Mn(Cl)(CO)$_3$(L-L)]$^+$ results in a dissociative bond-rupture mechanism. In this case $\Delta S^{\ddagger}$ significantly increased on replacement of chloride by bromide [16].

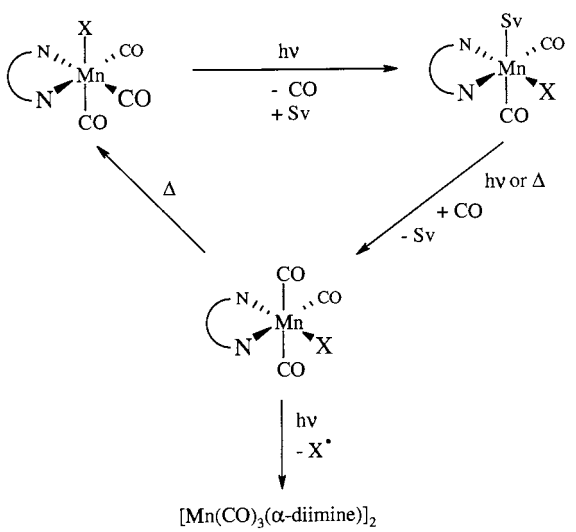

Scheme 1. Mechanism of the photoisomerization of *fac*-[Mn(X)(CO)$_3$(α-diimine)].

A twist-mechanism has also been proposed for the *fac*-to-*mer* isomerization of the complexes *fac*-[M(CO)$_3$(L)$_3$] (M = Cr, Mo, W; L = PR$_3$, P(OR$_3$), CNMe) [17]. The rate of isomerization was found to increase in the order Mo < W < Cr. In comparison with the Cr complexes, the W complexes isomerized more slowly due to more negative $\Delta S^{\ddagger}$ given by little lengthening of the W–P bond in the trigonal-prismatic transition state, whereas the kinetics of the Mo compounds was governed by higher activation enthalpy arising from the higher Mo–P enthalpy. The isomerization was also accelerated in the presence of more sterically demanding PR$_3$ ligands due to increasing relief of the interligand steric strain in the transition state.

In general, however, the trigonal-twist mechanism is rather uncommon in octahedral complexes containing monodentate ligands, in particular due to a high energetic barrier to intramolecular rearrangement with regard to a ground-state lengthening of the metal–ligand bonds (low activation enthalpy of ligand dissociation), which favours a dissocative process. The ligand size may influence both dissociative and trigonal-twist mechanisms [18].

In this paper, we present the results of a RT/FTIR study of the thermal *mer*-to-*fac* isomerization reaction of *mer*-[Mn(X)(CO)$_3$(α-diimine)]. Special attention has been paid to the determination of the activation enthalpy and entropy as a function of the nature of the bidentate α-diimine ligand, halide and the solvent used. The molecular structures of the *fac*- and *mer*-[Mn(X)(CO)$_3$(α-diimine)] complexes and the α-diimine ligands are schematically depicted in Fig. 1.

2. Experimental section

2.1. Materials and preparations

Tetrahydrofuran (THF; Janssen) and 2-methyl-tetrahydrofuran (2-MeTHF; Janssen) were dried on sodium wire. Acetonitrile (MeCN; Janssen) was refluxed with CaH$_2$. The solvents of spectrograde quality were distilled under a nitrogen atmosphere prior to use. The α-diimine ligands bpy′ (Fluka) and dpp (Aldrich) were used without further purification. The ligands *i*Pr-PyCa and R-DAB were synthesized according to literature procedures [19]. The complexes *fac*-[Mn(X)(CO)$_3$(α-diimine)] were prepared as previously described [20,21], with the modification that the reactants were refluxed in hexane for 3 h in the absence of

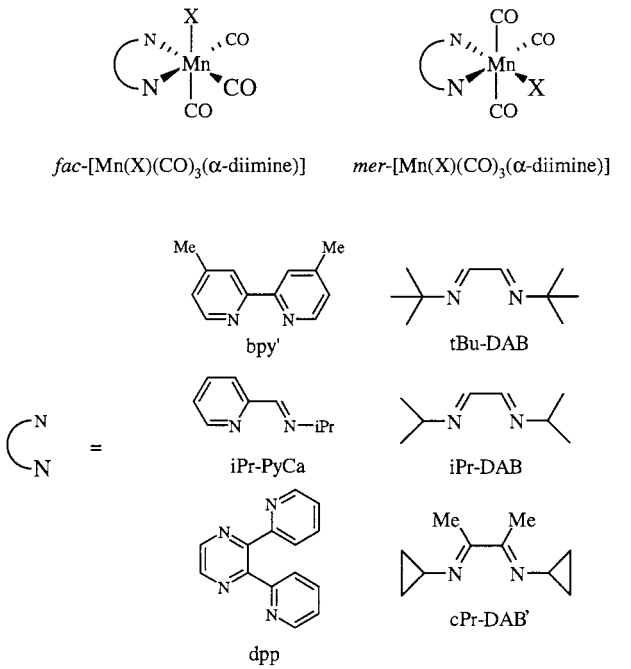

Fig. 1. General molecular structures of the complexes *fac*- and *mer*-[Mn(X)(CO)$_3$(α-diimine)] and the α-diimine ligands used.

light. The products were purified in the dark by column chromatography on activated silicagel (Kieselgel 60, Merck, 70–230 mesh), with a gradient elution of hexane/THF. All spectroscopic samples were prepared by standard inert gas techniques and were 10^{-2} M in *fac*-[Mn(X)(CO)$_3$(α-diimine)].

2.2. Instrumentation and spectroscopic measurements

All RT/FTIR kinetic runs of the thermal isomerization reactions were carried out with a Bio-Rad FTS 60A system equipped with a dual-source Digital Module 896 interferometer, a liquid-nitrogen-cooled MCT detector and KRS 5 filters in the sample compartment. The experimental setup used, as well as the method of data collection were as previously described [7].

Temperature control of the sample solution ($T \pm 0.1$ K) was achieved with an Oxford DN 1704/54 liquid-nitrogen cryostat which contained a home-built IR cell equipped with CaF_2 windows. The samples were irradiated inside the sample compartment of the spectrometer with the 488.0 nm line of a Spectra Physics 2025 Ar^+ laser. The irradiation interval was fixed by a computer-controlled mechanical shutter. The electronic absorption spectra were recorded on a Varian Cary 4E spectrophotometer.

3. Results

The electronic absorption spectra of *fac*-[Mn(X)(CO)$_3$(α-diimine)] (X = Br; α-diimine = bpy′, *i*Pr-PyCa and *i*Pr-DAB, and X = Cl, Br and I; α-diimine = *i*Pr-DAB) are presented in Figs. 2 and 3, respectively. The electronic absorption spectra of the corresponding *mer*-isomers (see Figs. 4 and 5) were recorded using the following procedure. The initial step, i.e. the *fac*-to-*mer* photoisomerization of *fac*-[Mn(X)(CO)$_3$(α-diimine)], was performed as described elsewhere [7]. The UV–vis absorption spectra of *mer*-[Mn(X)(CO)$_3$(α-diimine)] were obtained from the transient spectra, recorded immediately after the irradiation period, by correcting for the bleach of the *fac*-isomer.

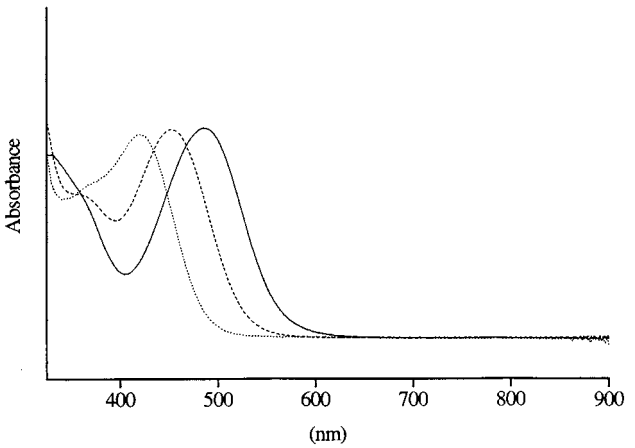

Fig. 2. Electronic absorption spectra of *fac*-[Mn(Br)(CO)$_3$(α-diimine)] (α-diimine = bpy′ (· · · ·), *i*Pr-PyCa (- - -) and *i*Pr-DAB (—)) in THF (293 K).

The ν(CO) wavenumbers of the photoproducts *mer*-[Mn(Br)(CO)$_3$(α-diimine)] and their parent *fac*-isomers are collected in Table 1. The reverse thermal isomerization of *mer*-[Mn(X)(CO)$_3$(α-diimine)] was followed by RT/FTIR spectroscopy, recording transient IR spectra within a time interval corresponding to the lifetime of the *mer*-isomer. Monitoring of the intensity of their middle ν(CO) bands at 1975–1945 cm^{-1} revealed an exponential decay of the photogenerated transients;

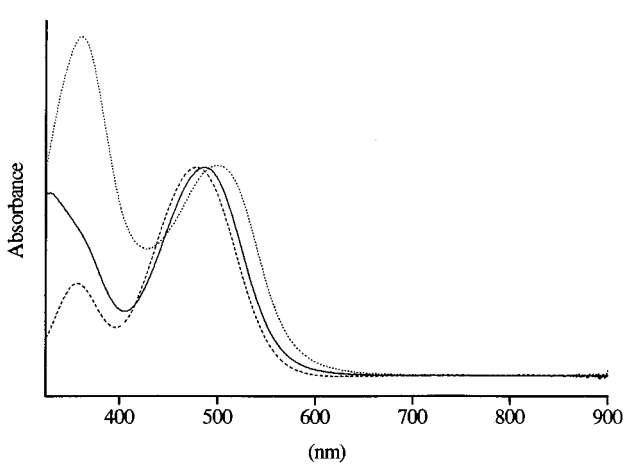

Fig. 3. Electronic absorption spectra of *fac*-[Mn(X)(CO)$_3$(*i*Pr-DAB)] (X = Cl (- - -), Br (—), I (· · · ·)) in THF (293 K).

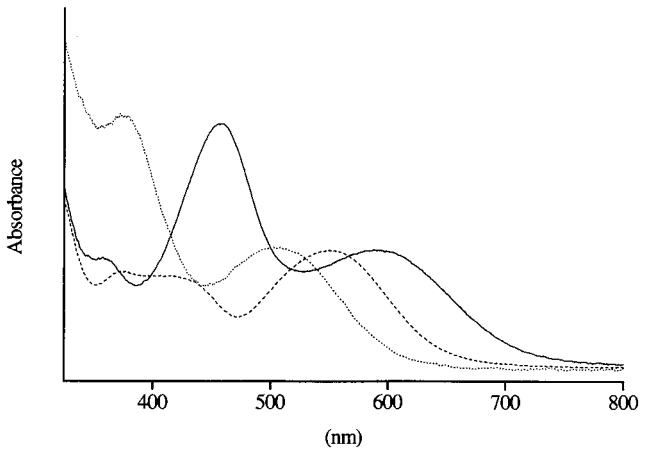

Fig. 4. Electronic absorption spectra of *mer*-[Mn(Br)(CO)$_3$(α-diimine)] (α-diimine = bpy′ (· · · ·), *i*Pr-PyCa (- - -) and *i*Pr-DAB (—)) in THF (273 K).

from good linear plots of $\ln(A_{oo}-A_t)$ versus time (pseudo)first-order rate constants were obtained (see Table 2).The reaction rates for the thermal isomerization of the *mer*-[Mn(X)(CO)$_3$(α-diimine)] complexes were found to rapidly decrease on lowering the temperature. Within the temperature range of 313–263 K the rate constants varied from 2 s^{-1} down to $1.25 \cdot 10^{-3}$ s^{-1}, depending on the solvent, the α-diimine and the halide ligands.

In the following step the thermodynamic activation parameters of the isomerization reaction $\Delta S^{\ddagger}$ and $\Delta H^{\ddagger}$, were obtained from Eyring plots (see Table 3). The rather large errors in $\Delta S^{\ddagger}$ are due to the small temperature range covered.

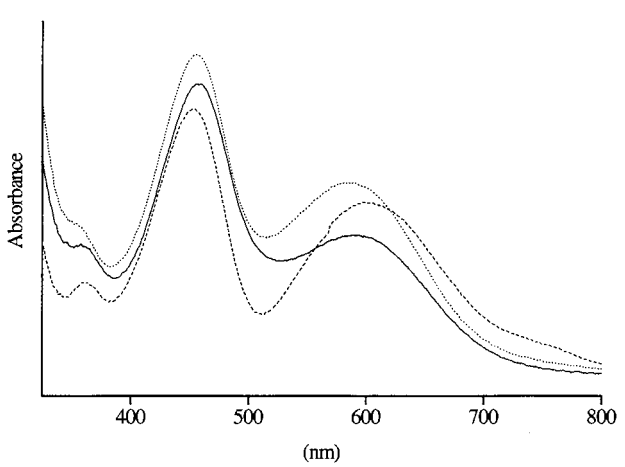

Fig. 5. Electronic absorption spectra of *mer*-[Mn(X)(CO)$_3$(*i*Pr-DAB)] (X = Cl (- - -), Br (—), I (· · · ·)) in THF (273 K).

4. Discussion

4.1. Electronic absorption spectra

The electronic absorption spectra of the *fac*- and *mer*-[Mn(X)(CO)$_3$(α-diimine)] complexes exhibit two dominant bands in the near-UV–vis region. Their positions strongly depend on the α-diimine ligand and the halide, and on the geometry. Varying the α-diimine ligand in *fac*-[Mn(Br)(CO)$_3$(α-diimine)] from *i*Pr-DAB to more basic *i*Pr-PyCa and bpy′ causes a shift of the lowest-lying absorption bands to higher energy. This result agrees with the increasing energy of the lowest π^*(α-diimine) orbital in the same order [22,23]. For the complexes *fac*-[Mn(X)(CO)$_3$(*i*Pr-DAB)] the intensity of the higher-lying absorption band increases with respect to that of the lower-energy one, on going from X = Cl, Br to I. In accordance with results of the spectroscopic and MO studies of [Mn(X)(CO)$_3$(α-diimine)] and closely related Ru-complexes [6,9,24], these two bands are assigned to charge transfer transitions from two sets of occupied orbitals possessing a metal (d_π)-halide (p_π) bonding- and antibonding character, respectively, to the mainly π^*(α-diimine) LUMO. In the case of the iodide complexes the iodide pπ orbitals contribute predominantly to the HOMO and HOMO-1 and the transitions of the lowest energy band therefore have mainly an iodide-to-α-diimine (L′LCT) character. The higher-energy electronic transitions exhibit a prevailing MLCT character.

The UV–vis spectra of *mer*-[Mn(Br)(CO)$_3$(α-diimine)] (α-diimine = bpy, *i*Pr-PyCa) have been reported by Stor et al. [6,25]. In Table 1 we present for the first time the UV–vis data for *mer*-[Mn(Br)(CO)$_3$(α-diimine)] (α-diimine = bpy′ and dpp) and *mer*-[Mn(X)(CO)$_3$(*i*Pr-DAB)] (X = Cl, Br, I). For all these complexes the lowest-lying visible absorption band possesses a lower intensity and a lower energetic position than found for their *fac*-isomers. Furthermore, this band shifts to lower energy with increasing π-acceptor capacity of the α-diimine ligand, identical as observed for the *fac*-isomers. These observations are in line with the bonding situation in *mer*-[Mn(Cl)(CO)$_3$(bpy)] described on the basis of density functional MO calculations [25] according to which the LUMO possesses a predominant π^*(α-diimine) character and the occupied antibonding MO combination of Mn (d_π) and halide (p_π) orbitals rises in energy relative to that of the *fac*-isomer.

The UV–vis spectra of *mer*-[Mn(X)(CO)$_3$(*i*Pr-DAB)] (X = Cl, Br, I) show hardly any influence of X. This result is rather unexpected in view of the decreasing ionization potentials of the halide p_π orbitals in the order Cl > Br > I. For X = I the lowest-energy electronic transition should therefore have the most pronounced L′LCT character [25] and the corresponding

Table 1
Infrared CO stretching frequencies and UV–vis data for *fac*- and *mer*-[Mn(X)(CO)$_3$(α-diimine)] at 293 K (unless stated otherwise)

Product	Solvent	ν(CO) (cm^{-1})	λ_{max} (nm)
fac-[Mn(Br)(CO)$_3$(bpy′)][b]	THF	2022 (s) 1933 (m) 1911 (m)	420
	CH_2Cl_2	2027 (s) 1932 (m) 1921 (m)	
fac-[Mn(Br)(CO)$_3$(dpp)][c]	THF	2026 (s) 1941 (m) 1922 (m)	460
fac-[Mn(Br)(CO)$_3$(*i*Pr-PyCa)][b]	THF	2023 (s) 1936 (m) 1915 (m)	452
fac-[Mn(Cl)(CO)$_3$(*i*Pr-DAB)]	THF	2024 (s) 1938 (m) 1917 (m)	478; 356
fac-[Mn(Br)(CO)$_3$(*i*Pr-DAB)][d]	THF	2023 (s) 1938 (m) 1918 (m)	485; 328
	CH_2Cl_2	2028 (s) 1943 (m) 1927 (m)	
	Toluene	2024 (s) 1944 (m) 1919 (m)	
fac-[Mn(I)(CO)$_3$(*i*Pr-DAB)]	THF	2023 (s) 1939 (m) 1919 (m)	501; 360
fac-[Mn(Br)(CO)$_3$(*t*Bu-DAB)][d]	THF	2020 (s) 1930 (m) 1917 (m)	
fac-[Mn(Br)(CO)$_3$(*c*Pr-DAB′)]	THF	2022 (s) 1940 (m) 1908 (m)	
mer-[Mn(Br)(CO)$_3$(bpy′)][b]	THF	2044 (w) 1945 (s) 1905 (m)	507; 376[a]
	CH_2Cl_2	2051 (w) 1951 (s) 1901 (m)	
mer-[Mn(Br)(CO)$_3$(dpp)][c]	THF	2051 (w) 1966 (s) 1916 (m)	560
mer-[Mn(Br)(CO)$_3$(*i*Pr-PyCa)][b]	THF	2046 (w) 1957 (s) 1911 (m)	550; 415[a]
mer-[Mn(Cl)(CO)$_3$(*i*Pr-DAB)]	THF	2051 (w) 1972 (s) 1918 (m)	600; 452[a]
mer-[Mn(Br)(CO)$_3$(*i*Pr-DAB)][d]	THF	2047 (w) 1967 (s) 1919 (m)	590; 455[a]
	CH_2Cl_2	2055 (w) 1976 (s) 1922 (m)	
	Toluene	2048 (w) 1974 (s) 1925 (m)	
mer-[Mn(I)(CO)$_3$(*i*Pr-DAB)]	THF	2047 (w) 1968 (s) 1920 (m)	584; 455[a]
mer-[Mn(Br)(CO)$_3$(*t*Bu-DAB)][d]	THF	2046 (w) 1961 (s) 1917 (m)	
mer-[Mn(Br)(CO)$_3$(*c*Pr-DAB′)]	THF	2038 (w) 1950 (s) 1916 (m)	

[a] T = 273 K.
[b] Ref. [6].
[c] Ref. [21].
[d] Ref. [7].

absorption band should shift to lower energy, as was found for the *fac*-isomers (see Fig. 3). Speculation of the significance of the above result does not seem warranted in the absence of comparative examples of *mer*-[Mn(X)(CO)$_3$(α-diimine)] (X = Cl, Br, I) complexes.

4.2. Isomerization of mer-[Mn(X)(CO)$_3$(α-diimine)]

In the previous section, we presented the kinetic data for the *mer*-to-*fac* isomerization of the complexes [Mn(X)(CO)$_3$(α-diimine)]. The effect of varying the α-diimine and halide ligands as well as the solvent on the mechanism of the isomerization reaction will now be discussed in more detail. The following characteristic features may be noted:

1. The enthalpy and entropy of activation for the isomerization of *mer*-[Mn(Br)(CO)$_3$(α-diimine)] strongly depend on the nature of the α-diimine ligand used. In THF, $\Delta H^{\ddagger}$ increases going from bpy′ to less basic *i*Pr-PyCa, *i*Pr-DAB and dpp, viz. from 63.1 to 75.1, 89.1 and 100.1 kJ·mol^{-1}, respectively. The values for $\Delta S^{\ddagger}$ also increase from −77 to −36, 29 and 133 J·mol^{-1}·K^{-1} [26].
2. A large solvent effect on $\Delta H^{\ddagger}$ and $\Delta S^{\ddagger}$ has been found for the complex *mer*-[Mn(Br)(CO)$_3$(bpy′)], while for corresponding *mer*-[Mn(Br)(CO)$_3$(*i*Pr-DAB)] hardly any influence of the solvent has been observed.
3. For the halide complexes *mer*-[Mn(X)(CO)$_3$(*i*Pr-DAB)] (X = Cl, Br) similar values for $\Delta H^{\ddagger}$ and $\Delta S^{\ddagger}$ have been determined while for X = I both activation parameters, in particular $\Delta S^{\ddagger}$, are lower.
4. Steric demands of the substituents on the α-diimine ligand are not important in the series of the complexes *mer*-[Mn(Br)(CO)$_3$(R-DAB)] (R = *c*Pr, *i*Pr and *t*Bu), for $\Delta H^{\ddagger}$ and $\Delta S^{\ddagger}$ are rather similar and show no consistent trends [26].

The activation parameters presented in Table 3 reveal that the complexes *mer*-[Mn(Br)(CO)$_3$(α-diimine)] can be divided with regard to the mechanism of their *mer*-to-*fac* isomerization in THF into two principal groups:

1. The complexes with the R-DAB and dpp ligands whose isomerization is characterized by $\Delta H^{\ddagger}$ = 80–100 kJ·mol^{-1} and positive $\Delta S^{\ddagger}$ values.
2. The complexes with the more basic bpy′ and *i*Pr-PyCa ligands. In this case $\Delta H^{\ddagger}$ = 60–75 kJ·mol^{-1} and $\Delta S^{\ddagger}$ is negative. The complex *mer*-[Mn(I)(CO)$_3$(*i*Pr-DAB)] also belongs to this group.

Angelici et al. showed that the *fac*-to-*mer* isomerization of *fac*-[Mn(Br)(CO)$_3$(PR$_3$)$_2$] involves rupture of a Mn–P bond [15]. The values for $\Delta H^{\ddagger}$ were found in this case to range between 110–130 kJ·mol^{-1}, depending on the nature of the phosphine ligands. In all of these

Table 2
(Pseudo)first-order rate constant (s^{-1})[a] for the *mer*-to-*fac* isomerization of *mer*-[Mn(X)$(CO)_3$(α-diimine)] at variable temperatures[b] in THF (unless stated otherwise)

α-diimine	bpy′	bpy′[c]	dpp	*i*Pr-PyCa	*i*Pr-DAB	*i*Pr-DAB	*i*Pr-DAB	*i*Pr-DAB[c]	*i*Pr-DAB[d]	*c*Pr-DAB′	*t*Bu-DAB
X (K)	Br	Br	Br	Br	Cl	Br	I	Br	Br	Br	Br
313	$2.14\cdot10^{-2}$ (3.3)	$1.32\cdot10^{-2}$ (3.9)									
308	$9.77\cdot10^{-3}$ (3.9)	$6.91\cdot10^{-3}$ (0.6)	$6.80\cdot10^{-3}$ (0.2)								
303	$5.28\cdot10^{-3}$ (8.4)	$3.65\cdot10^{-3}$ (0.8)	$3.55\cdot10^{-3}$ (3.0)	$9.07\cdot10^{-3}$ (4.2)							
298	$4.71\cdot10^{-3}$ (8.0)	$2.23\cdot10^{-3}$ (3.5)	$1.86\cdot10^{-3}$ (3.7)	$5.22\cdot10^{-3}$ (11.6)							
293	$3.75\cdot10^{-3}$ (6.1)	$1.28\cdot10^{-3}$ (9.1)	$1.07\cdot10^{-3}$ (12.6)	$3.28\cdot10^{-3}$ (4.2)	$1.59\cdot10^{-1}$ (11.1)	$2.95\cdot10^{-2}$ (10.9)	$1.35\cdot10^{-2}$ (2.2)	$1.80\cdot10^{-2}$ (1.0)	$6.41\cdot10^{-2}$ (1.3)		$8.33\cdot10^{-1}$ (1.2)
288	$2.08\cdot10^{-3}$ (9.2)			$1.78\cdot10^{-3}$ (5.5)	$1.45\cdot10^{-1}$ (9.9)	$1.34\cdot10^{-2}$ (1.2)	$7.91\cdot10^{-3}$ (4.0)	$9.24\cdot10^{-3}$ (3.2)	$3.21\cdot10^{-2}$ (2.1)		$4.35\cdot10^{-1}$ (5.2)
283	$1.24\cdot10^{-3}$ (9.8)			$1.06\cdot10^{-3}$ (0.1)	$5.52\cdot10^{-2}$ (12.4)	$6.67\cdot10^{-3}$ (2.0)	$4.60\cdot10^{-3}$ (12.4)	$4.20\cdot10^{-3}$ (4.5)	$1.53\cdot10^{-2}$ (2.0)	2.17 (7.4)	$2.17\cdot10^{-1}$ (5.9)
278					$2.67\cdot10^{-2}$ (5.9)	$3.53\cdot10^{-3}$ (0.7)	$2.60\cdot10^{-3}$ (6.0)	$2.37\cdot10^{-3}$ (1.8)	$7.47\cdot10^{-3}$ (0.3)	$9.71\cdot10^{-1}$ (5.0)	$1.15\cdot10^{-1}$ (2.5)
273					$1.31\cdot10^{-2}$ (0.7)	$1.84\cdot10^{-3}$ (4.6)	$1.40\cdot10^{-3}$ (2.3)	$1.10\cdot10^{-3}$ (1.0)	$3.75\cdot10^{-3}$ (7.9)	$5.24\cdot10^{-1}$ (2.5)	$5.75\cdot10^{-2}$ (0.1)
268										$2.60\cdot10^{-1}$ (1.4)	
263										$1.20\cdot10^{-1}$ (0.6)	

[a] Standard deviation (in %) in parentheses.
[b] $T\pm0.1$ K.
[c] In CH_2Cl_2.
[d] In toluene.

Table 3
Activation parameters[a,b] for the formation of *fac*-[Mn(X)(CO)$_3$(α-diimine) from *mer*-[Mn(X)(CO)$_3$(α-diimine)]

α-diimine	X	Sv	$\Delta H^{\ddagger}$	$\Delta S^{\ddagger}$
bpy′	Br	THF	63 ± 9.8	-77 ± 33
bpy′	Br	CH_2Cl_2	85.7 ± 6.0	-7 ± 20
dpp	Br	THF	100.0 ± 3.3	133 ± 11
*i*Pr-PyCa	Br	THF	75.1 ± 3.2	-36 ± 11
*i*Pr-DAB	Cl	THF	82.3 ± 7.3	21 ± 26
*i*Pr-DAB	Br	THF	89.1 ± 6.8	29 ± 24
*i*Pr-DAB	I	THF	72.8 ± 3.7	-32 ± 12
*i*Pr-DAB	Br	CH_2Cl_2	90.1 ± 3.9	29 ± 14
*i*Pr-DAB	Br	Toluene	92.4 ± 2.9	47 ± 10
*c*Pr-DAB′	Br	THF	86.4 ± 2.9	67 ± 11
*t*Bu-DAB	Br	THF	86.5 ± 1.6	49 ± 6

[a] $\Delta H^{\ddagger}$ in kJ·mol^{-1}; $\Delta S^{\ddagger}$ in J·mol^{-1}·K^{-1}.
[b] Error based on 95% confidence interval.

cases positive values for $\Delta S^{\ddagger}$ were determined. In contrast to this, the activation enthalpy is about three times lower for the probably non-dissociative ($\Delta S^{\ddagger} < 0$) *fac*-to-*mer* isomerization of *fac*-[Mn(Br)(CO)$_3$(P-P)]$^+$ (P-P = bidentate phosphine) [16]. Notably, for the Mn–X bonds in [Mn(X)(CO)$_5$] (X = Cl, Br, I) bond enthalpies of 294, 242 and 195 kJ·mol^{-1}, respectively, have been obtained from thermochemical studies [27]. For the complexes [Mn(Cl)(CO)$_5$] the measured mean thermochemical M–CO bond dissociation energy is 115 kJ·mol^{-1} [28].

From our data it is evident that the *mer*-to-*fac* isomerization of the complexes *mer*-[Mn(X)(CO)$_3$(α-diimine)] under study is an intricate process. Its course is mainly determined by the electronic properties of the α-diimine ligand and cannot be described with a single general mechanism. We, therefore, prefer to discuss the individual cases separately.

The complexes *mer*-[Mn(X)(CO)$_3$(R-DAB)] (X = Br, R = *c*Pr, *i*Pr, *t*Bu; X = Cl, R = *i*Pr) are kinetically most labile. The positive $\Delta S^{\ddagger}$ values indicate a dissociative mechanism involving a pseudopentacoordinate intermediate. The relatively small $\Delta H^{\ddagger}$ values do not favour cleavage of the Mn–Br bond in view of the likely much higher Mn–Br bond enthalpy (see above). The rather limited solvent dependence of $\Delta H^{\ddagger}$ and $\Delta S^{\ddagger}$ for *mer*-[Mn(Br)(CO)$_3$(*i*Pr-DAB)] (see Table 3) is not expected for a reaction course involving a cleavage of a Mn–CO bond. We therefore propose that the key step in the isomerization mechanism is the cleavage of a Mn–N bond giving rise to monodentate σ,*N*-coordination of the R-DAB ligand, followed by rapid intramolecular rearrangement to the *fac*-geometry. Such a reactivity of the highly flexible nonaromatic R-DAB ligands is not surprizing. For example, photochemical CO substitution reactions of the complexes [Fe(CO)$_3$(R-DAB)] also proceeded via partial dissociation of the R-DAB ligands, yielding intermediates with σ,*N*-coordinated R-DAB in their *trans*-isomeric form. For the derivatives [Fe(CO)$_3$(α-diimine)] (α-diimine = bpy, R-PyCa) the formation of the corresponding σ,*N*-monodentate intermediates was postulated to have much higher activation barrier [29].

The *mer*-to-*fac* isomerization of *mer*-[Mn(Br)(CO)$_3$(dpp)] with the rather strong π-acceptor dpp ligand obviously also follows a bond-breaking path, as evidenced by the positive $\Delta S^{\ddagger}$ value. In this case we may reasonably expect that the electron-withdrawing character of the uncoordinated nitrogen sites of the dpp ligand (see Fig. 1) results in reduced N → Mn σ-donation, making the Mn–N bonds prone to break more easily than on coordination of the stronger σ-donor bpy′ ligand (see below). The dpp ligand is larger and more rigid than R-DAB, which may explain the larger $\Delta S^{\ddagger}$ value relative to those for *mer*-[Mn(Br)(CO)$_3$(R-DAB)]. The larger $\Delta H^{\ddagger}$ value may reflect the higher thermodynamic stability of *mer*-[Mn(Br)(CO)$_3$(dpp)] caused by the larger steric demands of the σ,*N*-coordinated dpp ligand in the transition state. As a result, the latter complex is kinetically considerably less labile than the R-DAB-derivatives, in particular *mer*-[Mn(Br)(CO)$_3$(*c*Pr-DAB′)] (see Table 2).

Considering the *mer*-to-*fac* isomerization of *mer*-[Mn(Br)(CO)$_3$(bpy′)] in THF, the negative $\Delta S^{\ddagger}$ term and apparently smaller $\Delta H^{\ddagger}$ component in this case may be indicative of gross reorganization in the transition state without metal-ligand bond cleavage. The smaller rate constant for this reaction in CH_2Cl_2 reveals, however, a non-negligible rate-accelerating effect of THF. The considerably more negative value for $\Delta S^{\ddagger}$ determined in the latter solvent implies a mechanism in which THF is involved in the transition state. The strong solvent dependence thus excludes a simple trigonal–prismatic twist with little metal–ligand bond weakening in the transition state. A partial dissociation of the bromide ligand can be a more appropriate explanation. Due to a weaker Mn → bpy′ π-backdonation and a stronger σ-donation by the bpy′ ligand, the electron density on the metal increases relative to that in analogous R-DAB complexes. This strengthens the π-backdonation to the CO ligands, resulting in a significant decrease of CO stretching frequencies on going from *i*Pr-DAB to bpy′ (see Table 1). As a consequence of the increased charge on the Mn centre the Mn–X bond will be elongated, considering the Mn–X antibonding character of the HOMO and HOMO-1 [25]. The smaller $\Delta H^{\ddagger}$ and negative $\Delta S^{\ddagger}$ values for the isomerization of *mer*-[Mn(Br)(CO)$_3$(bpy′)] are consistent with an ionic mechanism, viz. dissociation of Br$^-$. For, an increase in the charge of the product probably requires increased electrostriction of the solvent and a

negative value for $\Delta S^{\ddagger}$ [30]. For *mer*-[Mn(Br)$(CO)_3$(α-diimine)] (α-diimine = R-DAB, dpp) the stronger Mn → α-diimine π-backdonation stabilizes the Mn–Br bond and prevents the solvent to participate in the transition state. A similar difference in reaction mechanisms has been reported by Delis et al. for isocyanide insertion into the Pd–Me bond of the complexes [Pd(Me)(Cl)(α-diimine)] (α-diimine = 2,2′-bipyridine (bpy) and 2,2′-bipyrimidine (bpym)) [31]. The initial step in this case involves coordination of the isocyanide to the Pd centre. The following step for the strongly σ-donating bpy ligand is dissociation of the chloride atom followed by migration of the methyl group to the isocyanide ligand. For the bpym ligand, whose electronic properties are comparable with those of the dpp and *i*Pr-DAB ligands [32–34], a different mechanism operates, involving Pd–N bond breaking instead of cleavage of the Pd–Cl bond.

In very weakly coordinating CH_2Cl_2 the Mn–N bond-rupture isomerization mechanism, proposed for *mer*-[Mn(Br)$(CO)_3$(α-diimine)] (α-diimine = R-DAB, dpp) (see above), probably becomes more important for *mer*-[Mn(Br)$(CO)_3$(bpy′)], resulting in larger values for $\Delta S^{\ddagger}$ and $\Delta H^{\ddagger}$ and decreased kinetic lability (see Tables 2 and 3). This trend toward the latter mechanism is also apparent for *mer*-[Mn(Br)$(CO)_3$(*i*Pr-PyCa)] which contains the less basic and more flexible *i*Pr-PyCa ligand with one reactive C=N imine bond. The *mer*-to-*fac* isomerization of the latter complex in THF is twice slower than that of the bpy′-derivative, but still significantly faster than that of the dpp-derivative. The negative value for $\Delta S^{\ddagger}$, however, implies that the solvent-assisted isomerization of *mer*-[Mn(Br)$(CO)_3$-(*i*Pr-PyCa)] in THF remains the major pathway.

The isomerization mechanism of *mer*-[Mn(I)$(CO)_3$(*i*Pr-DAB)] in THF deviates from that of the Cl- and Br-derivatives, as revealed by the negative value for $\Delta S^{\ddagger}$, smaller $\Delta H^{\ddagger}$ term and slower kinetics. We assume that in this case a mechanism related to that of *mer*-[Mn(Br)$(CO)_3$(bpy′)] plays a dominant role, probably due to the weaker Mn–X bond.

5. Conclusions

The kinetic and thermodynamic data clearly show that the mechanism and kinetics of the thermal *mer*-to-*fac* isomerization of *mer*-[Mn(X)$(CO)_3$(α-diimine)] (X = halide) strongly depend on the electronic and steric properties of the α-diimine ligands. For the complexes *mer*-[Mn(X)$(CO)_3$(α-diimine)] (X = Br, α-diimine = R-DAB, dpp; X = Cl, α-diimine = *i*Pr-DAB) the first reaction step involves cleavage of a Mn–N bond. The isomerization reaction is considerably slower for the large and rigid dpp ligand. On the other hand, *mer*-[Mn(Br)$(CO)_3$(α-diimine)] with stronger σ-donor bpy′ and *i*Pr-PyCa ligands and *mer*-[Mn(I)$(CO)_3$(*i*Pr-DAB)] with a weaker Mn–I bond, probably isomerize via a partial dissociation of the halide ligand. This path is particularly favoured in coordinating solvents like THF.

Acknowledgements

Thanks are due to the Netherlands Foundation for Chemical Research (SON) and the Netherlands Organization for the Advancement of Pure Research (NWO) for their financial support.

References

[1] D.J. Stufkens, Comments Inorg. Chem. 13 (1992) 359.
[2] T.A. Perkins, W. Humer, T.L. Netzel, K.S. Schanze, J. Phys. Chem. 94 (1990) 2229.
[3] P. Chen, T.D. Westmoreland, E. Danielson, K.S. Schanze, D. Anthon, P.E. Neveux Jr., T.J. Meyer, Inorg. Chem. 26 (1987) 1116.
[4] K.S. Schanze, D.B. MacQueen, T.A. Perkins, L.A. Cabana, Coord. Chem. Rev. 122 (1993) 63.
[5] L.A. Worl, R. Duesing, P. Chen, L.D. Ciana, T.J. Meyer, J. Chem. Soc. Dalton Trans. (1991) 849.
[6] G.J. Stor, S.L. Morrison, D.J. Stufkens, A. Oskam, Organometallics 13 (1994) 2641.
[7] C.J. Kleverlaan, F. Hartl, D.J. Stufkens, J. Photochem. Photobiol. A 203 (1997) 231.
[8] B.D. Rossenaar, D.J. Stufkens, A. Oskam, J. Fraanje, K. Goubitz, Inorg. Chim. Acta 247 (1996) 215.
[9] A. Rosa, G. Ricciardi, E.J. Baerends, D.J. Stufkens, J. Phys. Chem. 100 (1996) 15346.
[10] J.C. Bailar, Inorg. Nucl. Chem. 8 (1958) 165.
[11] P. Rây, N.K. Dutt, J. Indian Chem. 20 (1943) 81.
[12] C.S. Springer, R.E. Sievers, Inorg. Chem. 6 (1967) 852.
[13] R. Hoffman, J.M. Howell, A.R. Rossi, J. Am. Chem. Soc. 98 (1976) 2484.
[14] J.K. Burdett, Inorg. Chem. 15 (1976) 212.
[15] R.J. Angelici, F. Basolo, A.J. Poë, J. Am. Chem. Soc. 85 (1963) 2215.
[16] A.M. Bond, B.S. Grabaric, J.J. Jackowski, Inorg. Chem. 17 (1978) 1013.
[17] J.A.S. Howell, P.C. Yates, N.F. Ashford, D.T. Dixon, R. Warren, J. Chem. Soc. Dalton Trans. (1996) 3959.
[18] W.L. Ingham, N.J. Covill, Organometallics 11 (1992) 2551.
[19] H. Bock, H. tom Dieck, Chem. Ber. 100 (1967) 228.
[20] L.H. Staal, A. Oskam, K. Vrieze, J. Organomet. Chem. 170 (1979) 235.
[21] J.W.M. van Outersterp, Ph.D. Thesis, University of Amsterdam, 1995.
[22] D.J. Stufkens, Coord. Chem. Rev. 104 (1990) 39.
[23] J. Reinhold, R. Benedix, P. Birner, H. Hennig, Inorg. Chim. Acta 33 (1979) 209.
[24] H.A. Nieuwenhuis, D.J. Stufkens, A. Vlček Jr., Inorg. Chem. 34 (1995) 3879.
[25] G.J. Stor, D.J. Stufkens, P. Vernooijs, E.J. Baerends, J. Fraanje, K. Goubitz, Inorg. Chem. 34 (1995) 1588.

[26] Attempts to extend the investigated series of the complexes *mer*-[Mn(X)(CO)$_3$(α-diimine)] with those containing bulky and electron-withdrawing R-DAB ligands, R = *p*-tolyl and *p*-anisyl, failed due to decomposition of parent fac-isomers during irradiation.
[27] J.A. Connor, M.T. Zafarani-Moattar, J. Bickerton, N.I. El Saied, S. Suradi, R. Carson, G. Al Takhin, H.A. Skinner, Organometallics 1 (1982) 1166.
[28] R.J. Angelici, F. Basolo, J. Am. Chem. Soc. 84 (1962) 2495.
[29] M.W. Kokkes, D.J. Stufkens, A. Oskam, J. Chem. Soc. Dalton Trans. (1984) 1005.
[30] G. Lappin (Ed.), Redox Mechanisms in Inorganic Chemistry, Ellis Horwood, Sussex, 1994.
[31] J.G.P. Delis, P.G. Aubel, K. Vrieze, P.W.N.M. van Leeuwen, N. Veldman, A.L. Spek, F.J.R. van Neer, Organometallics 16 (1997) 2948.
[32] G.J. Stor, F. Hartl, J.W.M. van Outersterp, D.J. Stufkens, Organometallics 14 (1995) 1115.
[33] J.W.M. van Outersterp, F. Hartl, D.J. Stufkens, Organometallics 14 (1995) 3303.
[34] B.D. Rossenaar, F. Hartl, D.J. Stufkens, Inorg. Chem. 35 (1996) 6194.